DOI: 10.1002/ejic.201100848

Cell Cycle Arrest, Cytotoxicity, Apoptosis, DNA-Binding, Photocleavage, and Antioxidant Activity of Octahedral Ruthenium(II) Complexes

Hong-Liang Huang,[a] Zheng-Zheng Li,[b] Zhen-Hua Liang,[b] and Yun-Jun Liu*[b]

Keywords: Bioinorganic chemistry / Medicinal chemistry / Cytotoxicity / Apoptosis / Cell cycle / Ruthenium

Three ruthenium(II) complexes $[Ru(dmp)_2(dcdppz)]^{2+}$ **1**, $[Ru(phen)_2(dcdppz)]^{2+}$ **2**, and $[Ru(dip)_2(dcdppz)]^{2+}$ **3** were synthesized and characterized. The crystal structure of complex **1** was solved by single-crystal X-ray diffraction. This complex crystallizes in the monoclinic system, space group *C*2/*c* with a = 18.454(3) Å, b = 44.648(7) Å, c = 13.082(2) Å, β = 99.911(3)°, R = 0.0571, and R_ω = 0.1501. The DNA-binding constants were determined to be 1.78 ($\pm$0.24) $\times 10^5$, 2.73 ($\pm$0.16) $\times 10^5$, and 7.55 ($\pm$0.16) $\times 10^5$ M^{-1} for **1**, **2**, and **3**, respectively. The photocleavage of pBR322 DNA by Ru^{II} complexes was studied. The retardation assay of pGL 3 plasmid DNA was investigated. The cytotoxicity of complexes **1**, **2**, and **3** against BEL-7402, Hela, HepG-2, and MG-63 cells was evaluated by the MTT method. Complexes **1** and **3** show higher cytotoxicity than Cisplatin on Hela cells. The apoptosis and cell cycle arrest were investigated, and the antioxidant activities of these complexes were also explored.

Introduction

The interaction of ruthenium complexes with DNA has been a topic of major bioinorganic interest during the past decades. Ruthenium complexes containing dppz have been extensively studied.[1–6] As a star molecule, complex $[Ru(bpy)_2(dppz)]^{2+}$ (dppz = dipyrido[3,2-*a*:2′,3′-*c*]phenazine) can serve as a prominent molecular "light switch," which shows no luminescence in aqueous solution at ambient temperature, but luminesces brightly upon binding intercalatively with the dppz ligand between the adjacent DNA base pairs. In recent years great attention has been given to studies of the bioactivity of ruthenium(II) complexes. Complex $[Ru(dip)_2(1\text{-Py-}\beta C)]^{2+}$ {1-Py-βC = 1-(2-pyridyl)-β-carboline} displayed activities greater than cisplatin on HepG-2, Hela, and MCF-7 cells.[7] Complex $[Ru(bpy)_2(dppn)]^{2+}$ exhibits high cytotoxicity against human MCF-7 cancer cell lines comparable to that of cisplatin.[3] Complex $[Ru(phen)_2(dppz)]^{2+}$ can bind to CT-DNA with a very large DNA-binding affinity ($>10^6$ M^{-1}), and can inhibit proliferation of MCF-7 cells to a moderate degree.[3] However, the derivatives of dppz have been given little attention. To obtain more insight into derivatives of ruthenium(II) complexes containing dppz and their interaction with DNA and bioactivity in vitro, in this article, a new ligand dcdppz and its three complexes $[Ru(dmp)_2$(dcd-

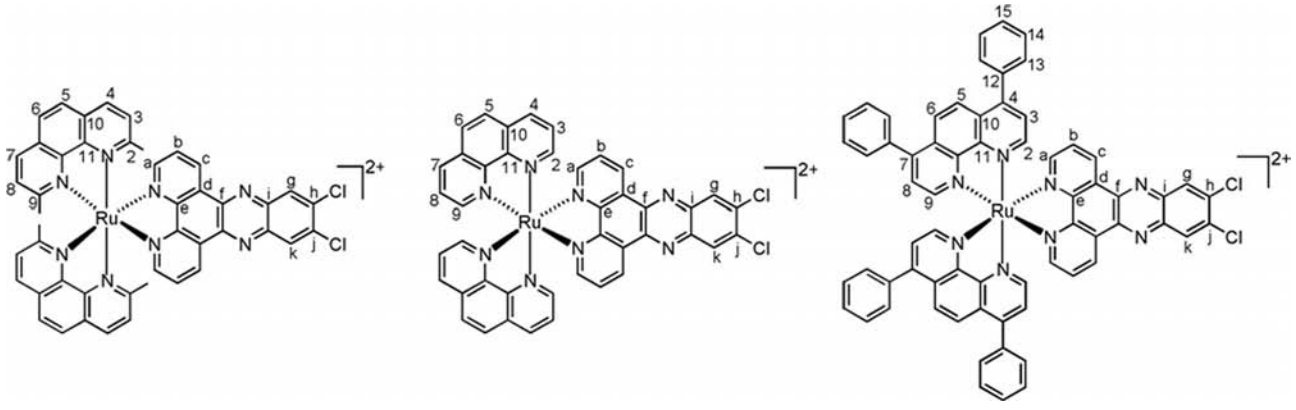

Scheme 1. The structure of complexes **1**, **2**, and **3**.

[a] School of Life Science and Biopharmaceutical, Guangdong Pharmaceutical University, Guangzhou, 510006, PR China
[b] School of Pharmacy, Guangdong Pharmaceutical University, Guangzhou, 510006, PR China
Fax: +86-20-39352128
E-mail: lyjche@163.com (Y.-J. Liu)

ppz)]$^{2+}$ **1** (dcdppz = 7,8-dichlorodipyrido[3,2-*a*:2′,3′-*c*]-phenazine, dmp = 2,9-dimethyl-1,10-phenanthroline), [Ru(phen)$_2$(dcdppz)]$^{2+}$ **2** (phen = 1,10-phenanthroline), and [Ru(dip)$_2$(dcdppz)]$^{2+}$ **3** (dip = 4,7-diphenyl-1,10-phenanthroline, Scheme 1) were synthesized and characterized. Their DNA-binding behaviors were studied by electronic absorption titration, viscosity measurements, and photoactivated cleavage. The results indicated that complexes **1**, **2**, and **3** can intercalate between the base pairs of DNA. The cytotoxicity of these complexes was evaluated by MTT {MTT = [3-(4,5-dimethylthiazol-2-yl)-2,5-diphenyltetrazolium bromide]} assay. The apoptosis of BEL-7402 cells induced by Ru^{II} complexes was also studied. The cell cycle arrest was analyzed by flow cytometry. The antioxidant activity of these complexes was explored by the hydroxy radical (˙OH) scavenging method in vitro.

Results and Discussion

Synthesis, Characterization, and Structure

The ligand dcdppz was synthesized by condensing 1,10-phenanthroline-5,6-dione and 4,5-dichloro-1,2-phenylenediamine in ethanol. The complexes **1**, **2**, and **3** were prepared by direct reaction of dcdppz with the appropriate precursor complexes in ethylene glycol in relatively high yield. The desired Ru^{II} complexes were isolated as the perchlorates and purified by column chromatography. The molecular structure of complex **1** was confirmed by single-crystal X-ray diffraction analysis. An ORTEP drawing of the cation with the atomic numbering scheme is depicted in Figure 1. Crystal data, selected bond lengths, and bond angles are collected in Table 4 and Table 1. Complex **1** consists of a [Ru(dmp)$_2$(dcdppz)]$^{2+}$ cation, two ClO_4^-, two CH_3CN molecules, and one and a half water molecules. The Ru^{II} center of complex **1** is chelated by two ancillary ligands dmp and an intercalative ligand dcdppz and adopts a distorted octahedral geometry, and the average Ru–N bond length is 2.085(3) Å, which is larger than that published for [Ru(phen)$_3$]$^{2+}$ (2.063 Å)[8] and comparable to those found for [Ru(dmp)$_2$(fpp)]$^{2+}$ (2.088 Å).[9] The dihedral angle between the two dmp planes is 67.6°. And the dihedral angle between the two ideal ring planes I (Cl$_1$, C$_{43}$, C$_{44}$, Cl$_2$) and II (C$_{41}$ to C$_{46}$) is 2.6°.

Table 1. Selected bond lengths [Å] and angles [°] for complex **1**.

Ru–N(1)	2.093(3)	Ru–N(4)	2.088(4)
Ru–N(2)	2.093(3)	Ru–N(5)	2.073(3)
Ru–N(3)	2.096(3)	Ru–N(6)	2.067(3)
N(1)–Ru–N(2)	79.52(13)	N(5)–Ru–N(6)	78.73(12)
N(1)–Ru–N(3)	178.53(13)	N(1)–Ru–C(1)	132.0(3)
N(1)–Ru–N(4)	102.33(14)	N(1)–Ru–C(12)	110.2(3)
N(1)–Ru–N(5)	81.16(13)	N(2)–Ru–C(10)	130.8(3)
N(1)–Ru–N(6)	97.24(13)	N(2)–Ru–C(11)	110.6(2)
N(2)–Ru–N(3)	101.43(12)	N(3)–Ru–C(15)	131.6(2)
N(2)–Ru–N(4)	94.93(12)	N(3)–Ru–C(26)	111.4(2)
N(2)–Ru–N(5)	93.59(12)	N(4)–Ru–C(24)	129.3(3)
N(2)–Ru–N(6)	172.09(11)	N(4)–Ru–C(25)	111.2(3)
N(3)–Ru–N(4)	78.74(12)	N(5)–Ru–C(29)	128.3(3)
N(3)–Ru–N(5)	97.64(12)	N(5)–Ru–C(40)	114.2(3)
N(3)–Ru–N(6)	81.67(12)	N(6)–Ru–C(38)	128.3(3)
N(4)–Ru–N(5)	171.25(13)	N(6)–Ru–C(39)	113.9(2)
N(4)–Ru–N(6)	92.81(12)		

Viscosity Measurements

To further clarify the interaction between the complexes and CT-DNA, viscosity measurements were carried out. The changes in relative viscosity of the DNA solution have been proved useful for the assignment of the mode of binding compounds to DNA. Intercalation of a ligand into DNA is known to cause a significant increase in the viscosity of a DNA solution because of the increase in the separation of the base pairs at the intercalation site and, hence, an increase in the overall DNA molecular length.[10] The relative change in viscosity was measured using CT-

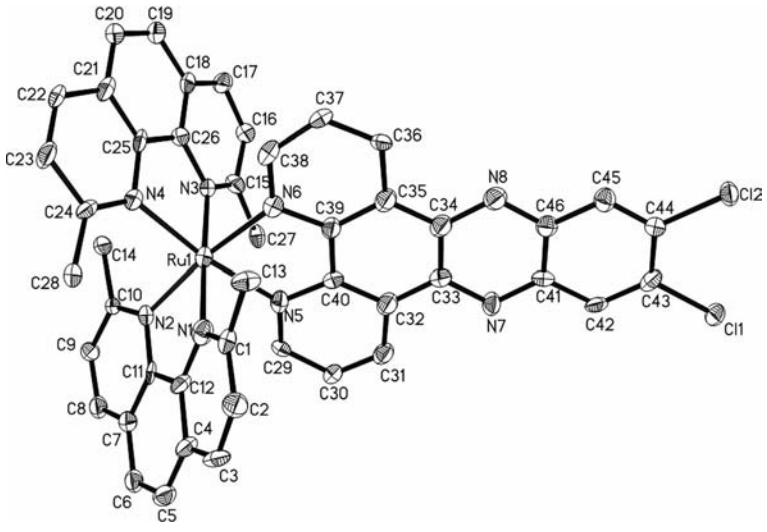

Figure 1. An ORTEP drawing of complex **1**.

DNA with increasing concentrations of the complexes **1**, **2**, and **3**. The effects of complexes **1**, **2**, and **3** on the relative viscosity of rod-like DNA are shown in Figure 2. Upon increasing the concentrations of complexes **1**, **2**, and **3** the relative viscosity of the DNA increased steadily following the order of complexes **3** > **2** > **1**. These results suggest that complexes **1**, **2**, and **3** intercalate between the base pairs of CT-DNA. The enhancements of the relative viscosity of DNA follow the order **3** > **2** > **1**, which is consistent with the DNA-binding affinities.

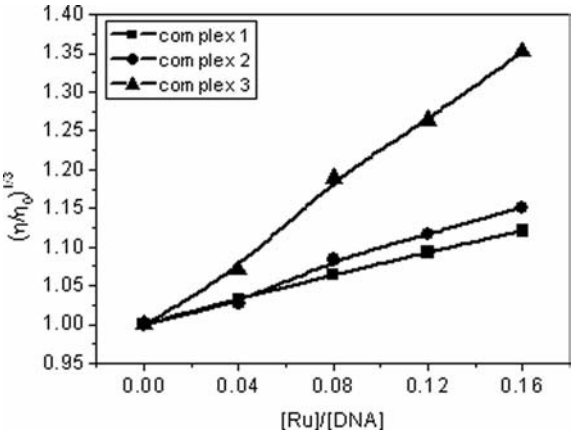

Figure 2. Effect of increasing amounts of complexes **1** (■), **2** (●), and **3** (▲) on the relative viscosity of calf thymus DNA at 25 (± 0.1) °C. [DNA] = 0.25 mM.

Electronic Absorption Spectra

The spectra of the three complexes consist of three or four well-resolved bands in the range of 200–600 nm. At the low energy band, all of them display a strong MLCT transition at 400–500 nm attributed to the overlap Ru(dπ)→dmp, phen, or dip (π*) and Ru(dπ)→dcdppz (π*). The spectra (300→390 nm) display a large change band, corresponding to (dcdppz)→π* and π→π* transitions. The band below 300 nm is attributed to intraligand (IL) transition by comparison with the spectrum of other polypyridyl Ru^{II} complexes.[11–13] The absorption spectra of complexes **1**, **2**, and **3** in the presence of increasing amounts of CT-DNA are shown in Figure 3. On increasing CT-DNA concentrations, the hypochromism of the MLCT band of **1** at 451 nm, **2** at 446 nm, and **3** at 452 nm upon binding to DNA was 32.17, 25.38, and 30.38%, respectively. These spectral characteristics obviously suggest that these complexes interact with DNA most likely through a mode that involves a stacking interaction between the aromatic chromophore and the base pairs of DNA.

To compare quantitatively the binding strength of these complexes, their intrinsic binding constants for binding with CT-DNA were obtained by monitoring the changes in absorbance at MLCT with increasing concentration of DNA. The intrinsic binding constants K_b of 1.78 $(\pm 0.24) \times 10^5$, 2.73 $(\pm 0.16) \times 10^5$, and 7.55 $(\pm 0.16) \times 10^5$ M^{-1} were obtained for complexes **1**, **2**, and **3**, respectively. These values are smaller than that of complexes $[Ru(bpy)_2(dppz)]^{2+}$ ($> 10^6$ M^{-1})[14] and $[Ru(bpy)_2(pddpz)]^{2+}$ {2.1 $(\pm 0.3) \times 10^6$ M^{-1}},[15] which may be caused by the two chlorine atoms in dppz reducing the intercalative degree of dppz between the DNA base pairs.

Luminescence and Continuous Variation Studies

Complex **1** cannot emit in Tris buffer at room temperature. Complexes **2** and **3** can emit with a maximum appearing at 601 and 610 nm for **2** and **3**, respectively. Figure 4 shows the emission spectra of complexes **2** and **3** in the presence of varying amounts of DNA. As seen from the figure the intensities of emission increase obviously in the presence of DNA. When the ratio of [DNA]/[Ru] reached a saturating value, the emission intensities of complexes **2** and **3** increased to 4.34 and 15.39 times the original intensities, respectively. The enhancement of emission intensity is indicative of binding of these complexes to the hydrophobic pocket of DNA.

Binding of complexes **2** and **3** to CT-DNA was examined at 25 °C in Tris-HCl buffer by the method of continuous variation analysis to determine the overall stoichiomet-

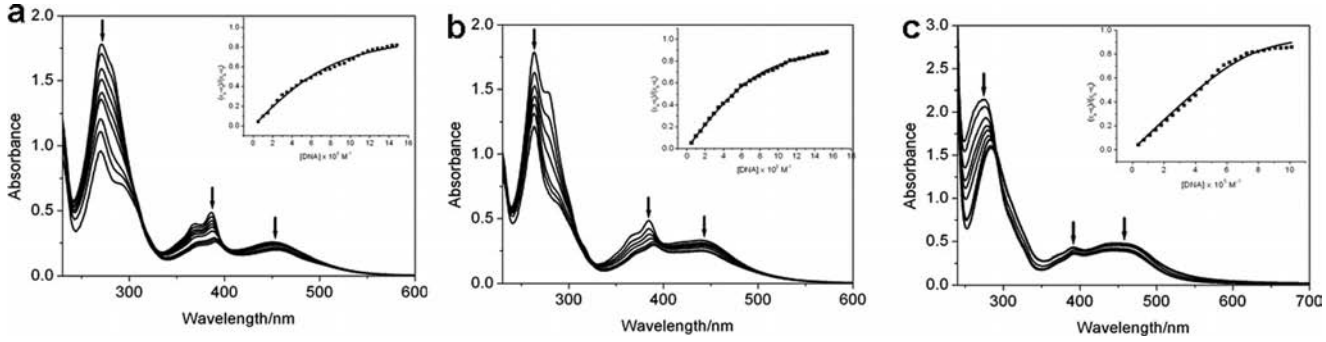

Figure 3. Absorption spectra of complexes **1** (a), **2** (b), and **3** (c) in Tris-HCl buffer upon addition of CT-DNA. [Ru] = 20 μM. Arrow shows the absorbance change upon the increase of DNA concentration. Plots of $(\varepsilon_a - \varepsilon_f)/(\varepsilon_b - \varepsilon_f)$ vs. [DNA] for the titration of DNA with Ru^{II} complexes.

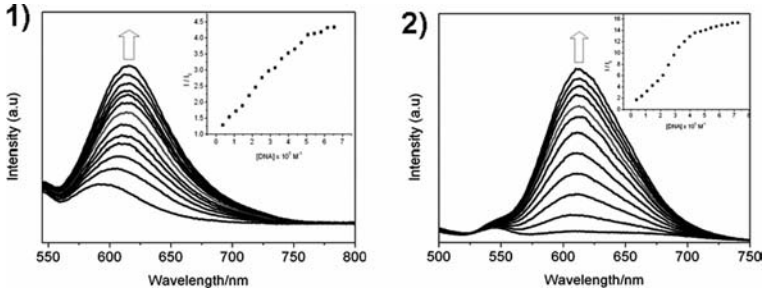

Figure 4. Emission spectra of complexes **2** (1) and **3** (2) in Tris-HCl buffer in the absence and presence of CT-DNA. Arrow shows the intensity change upon increasing DNA concentration. Inset: changes of intensity with increasing concentrations of CT-DNA.

ries.[16] The luminescence intensities of the Ru–DNA solution were recorded at 601 and 610 nm for complexes **2** and **3**, respectively. Figure 5 shows normalized Job plots for DNA. The point of intersection of two best-fit lines in the Job plots for complexes **2** and **3** with DNA are 0.29 and 0.30, which correspond to complex/DNA stoichiometries of 1:2 and 1:2, respectively.

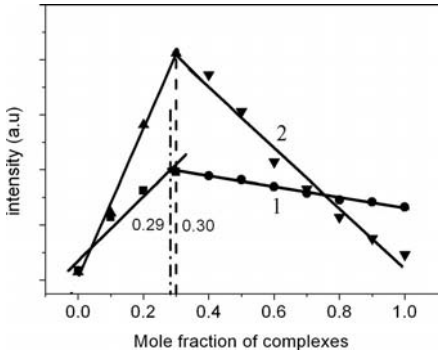

Figure 5. Job plot using luminescence data obtained at 601 and 610 nm for complexes **2** (1) and **3** (2) with CT-DNA in Tris-HCl buffer, respectively; pH = 7.0.

Photoinduced Cleavage of pBR322 DNA

When circular plasmid DNA is subjected to electrophoresis, relatively fast migration will be observed for the intact supercoiled form (Form I). If scission occurs on one strand (nicking), the supercoiled form will relax to generate a slower-moving open circular form (Form II).[17] Figure 6 shows gel electrophoresis separation of pBR322 DNA after incubation with different concentrations of complexes **1**, **2**, and **3** upon irradiation at 365 nm for 45 min. No obvious DNA cleavage was observed for the control in which the complex was absent (DNA alone), or incubation of the plasmid with the Ru^{II} complexes in the dark. At increasing concentration of the Ru^{II} complexes, the amount of Form I of pBR322 DNA diminishes gradually, whereas that of Form II increases. These results were also observed for other ruthenium(II) polypyridyl complexes.[18–20] Under the same experimental conditions, complexes **2** and **3** showed more effective DNA cleavage activity than complex **1**. The different cleaving efficiencies may be related to the different binding affinities of the three Ru^{II} complexes to DNA.

Ratardation of pGL 3 Plasmid DNA

Studies on cationic metal complexes condensing DNA have been given great attention. Complex $[Co(NH_3)_6]^{3+}$ condenses the plasmid pUC12, calf thymus DNA, λDNA, and polynucleotides into nanoparticles of 39–45 nm under neutral conditions.[21–23] Complexes $[Ru(bpy)_2(PIPSH)]^{2+}$[24] and $[Ru(phen)_2(DBHIP)]^{2+}$[25] can effectively condense DNA at room temperature. To evaluate their ability to condense DNA, gel retardation of pGL3 DNA was performed in the presence of different concentrations of complexes **1**, **2**, and **3**. Figure 7 shows that complexes **1**, **2**, and **3** cannot condense DNA at low concentrations (1 and 2 mM), however, effective condensation was observed when the concentrations of these complexes reached 3 and 4 mM.

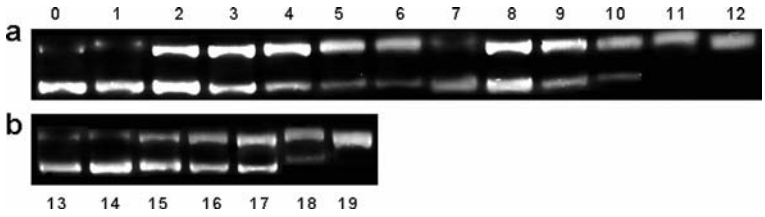

Figure 6. Photoactivated cleavage of pBR322 DNA in the presence of different complexes upon irradiation at 365 nm for 45 min. Lane 0, 13, DNA alone; a: lanes 1–6 for complex **1**: (1) 20 (in darkness); (2) 5; (3) 10; (4) 20; (5) 40; (6) 60 μM; lane 7–12 for complex **2**: (7) 20 (in darkness); (2) 5; (9) 10; (10) 20; (11) 40; (12) 60 μM; b: lane 14–19 for complex **3**: (14) 20 (in darkness); (15) 5; (16) 10; (17) 20; (18) 40; (19) 60 μM.

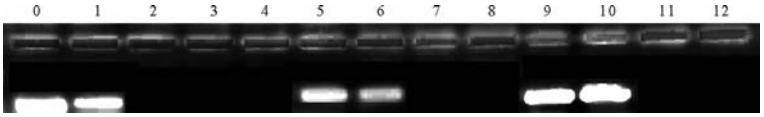

Figure 7. Agarose gel electrophoresis retardation of pGL3 plasmid DNA in the presence of different concentrations of complex **1**: Lane (0) DNA alone, (1) 1 mM, (2) 2 mM, (3) 3 mM, (4) 4 mM and complex **2**: (5) 1 mM, (6) 2 mM, (7) 3 mM, (8) 4 mM; complex **3**: (9) 1 mM, (10) 2 mM, (11) 3 mM, (12) 4 mM. [DNA] = 0.5 ng.

Cytotoxicity Assay in Vitro

The cytotoxicity of complexes **1**, **2**, and **3** to BEL-7402, Hela, HepG-2, and MG-63 was assayed by cell survival after 72 h of exposure to the desired concentration range (6.25→400 μM) using the MTT assay. The culture medium and cisplatin were used as the negative and positive controls, respectively. The IC_{50} values obtained are listed in Table 2, and the cell viability is depicted in Figure 8. The IC_{50} values for **1**, **2**, and **3** range from 12.31 to 27.33 μM. Comparing the IC_{50} values of these complexes, complex **3** shows higher activity on Hela and HepG-2 cells than complexes **1** and **2** under the same experimental conditions. This may be the result of an increase in lipophilicity caused by the substituent Ph in phen. Furthermore, complexes **1** and **3** displayed higher cytotoxicity than cisplatin to Hela cells. When compared with complex $[Ru(phen)_2(p\text{-}MOPIP)]^{2+}$, which shows high antiproliferative activity toward HepG-2 cells with a low IC_{50} value of 7.2 ± 1.2 μM,[26] complexes **1**, **2**, and **3** show low cytotoxicity. Figure 8 shows that cell viability was also found to be concentration dependent, and on increasing the concentration of complexes **1**, **2**, and **3**, an obvious decrease was observed in cell viability.

Table 2. The IC_{50} values of complexes **1**, **2**, and **3** against the selected cell lines.

	IC_{50} (μM) BEL-7402	Hela	HepG-2	MG-63
1	26.14 ± 2.26	13.79 ±2.12	27.33 ±3.25	22.51 ±1.35
2	16.90 ± 1.89	16.38 ±2.16	26.89 ±2.86	25.82 ±2.45
3	24.72 ±2.35	12.31 ±1.42	22.63 ±2.56	15.41 ±1.22
cisplatin	19.76 ±2.18	16.85 ±2.53	20.25 ±3.23	–

Apoptosis Studies

External aggression by a chemical compound sensed by the cells causes them to undergo two major forms of death, necrosis or apoptosis, each with very distinct characteristics. Cell necrosis is a consequence of the inability to maintain intracellular homeostasis, initiated by an imbalance of ions and water influx, which is followed by cell swelling and rupture of intracellular organelles. That in turn leads to final loss of cell integrity by disruption of the plasma membrane.[27] The assay of apoptosis induced by complex **3** was carried out with a staining method utilizing acridine orange (AO) and ethidium bromide (EB).[28] AO can pass through

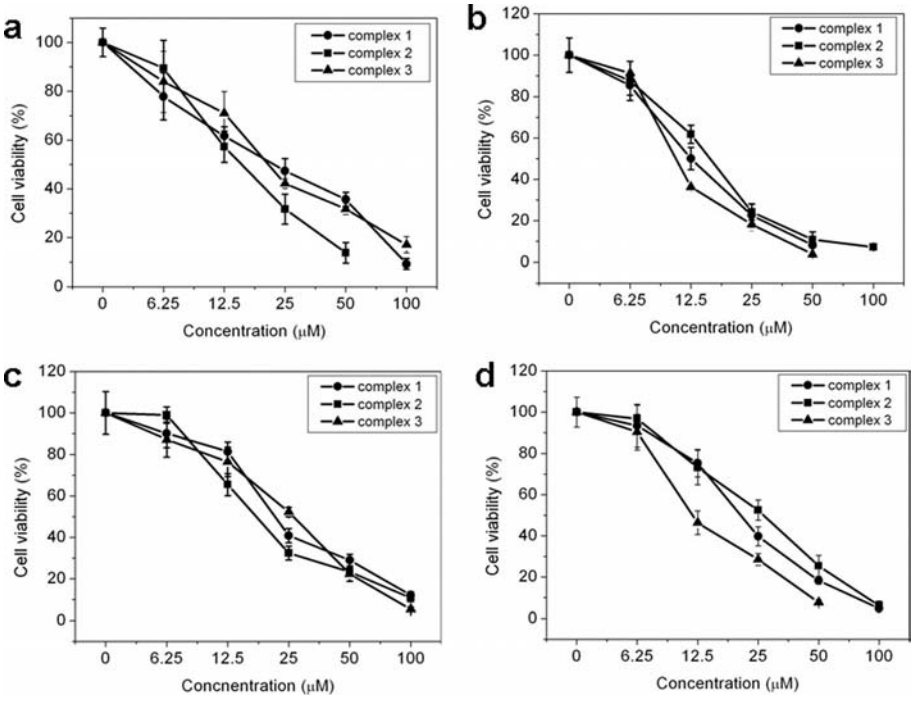

Figure 8. Cell viability of complexes **1**, **2**, and **3** on tumor BEL-7402 (a), Hela (b), HepG-2 (c) and MG-63 (d) cell proliferation in vitro. Each point is the mean ± standard error obtained from three independent experiments.

the cell membrane of living or early apoptotic cells, while staining by EB indicates loss of membrane integrity. Under the fluorescence microscope, living cells appear green, necrotic cells stain red but have a nuclear morphology resembling that of viable cells. In the absence of complex **3**, the living cells are stained bright green in spots (Figure 9, A). However, after treatment with complex **3** for 24 h, green apoptotic cells containing apoptotic bodies, as well as red necrotic cells, were also observed (Figure 9, B). Similar results were observed for complexes **1** and **2**.

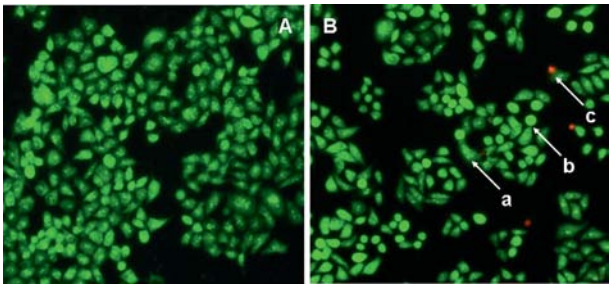

Figure 9. BEL-7402 cells were stained by AO/EB and observed under fluorescence microscopy. BEL-7402 cells without treatment (A) and in the presence of complex **3** (B, 25 μM) incubated at 37 °C and 5% CO_2 for 24 h. Cells marked by a, b, and c are living, apoptotic, and necrotic cells, respectively.

Cell Cycle Arrest by Flow Cytometry

The effect of complex **3** on the cell cycle of MG-63 cells was studied by flow cytometry in propidium iodide (PI)-stained cells after Ru^{II} complex treatment for 16 h. The representative DNA distribution histograms of MG-63 cells in the absence (a) and presence of different concentrations of complex **3** (b for 12.5 μM, c for 25 μM) is shown in parts a–c of Figure 10. When the concentration of complex **3** reached 25 μM, an obvious enhancement (5.77%) in the percentage of cells at G0/G1 phase was observed, accompanied by a corresponding reduction in the percentage of cells in the S phase. Figure 10 (b and c) shows that the concentration of the complex has a large influence on the cell cycle of MG-63 cells. On increasing the concentration of complex **3**, the percentage of MG-63 cells in the G0/G1 phase increased from 2.24 to 5.77%. These results indicate that the antiproliferative mechanism induced by complex **3** on MG-63 cells is G0/G1 phase arrest.

Antioxidant Activity Studies

The hydroxy radical (·OH) is one of the most reactive products of the reactive oxygen species (ROS), and may result in cell membrane disintegration, membrane protein damage, DNA mutation, and further initiate or propagate the development of many diseases.[29,30] The hydroxy radical (·OH) in aqueous media was generated by the Fenton system.[31] The antioxidant activities of complexes **1**, **2**, and **3** against the hydroxy radical were investigated as shown in Figure 11 and Table 3. The suppression ratio against ·OH was 2.65 to 75.18%, 3.86 to 71.81%, and 4.34 to 79.28% for complexes **1**, **2**, and **3**, respectively, which indicated that the suppression ratio increased with increasing sample concentration in the range 0.5–4.5 μM. Also the inhibitory effect of these Ru^{II} complexes on ·OH was found to be concentration dependent. Under the same conditions, complexes **1**, **2**, and **3** display adjacent antioxidant activity. This

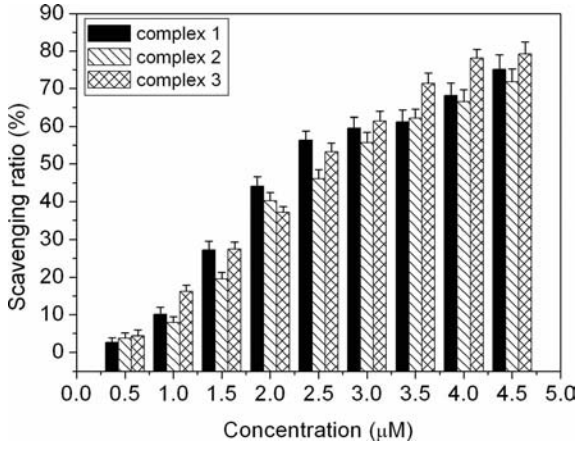

Figure 11. Scavenging effect of complexes **1**, **2** and **3** on hydroxy radicals. Experiments were performed in triplicate.

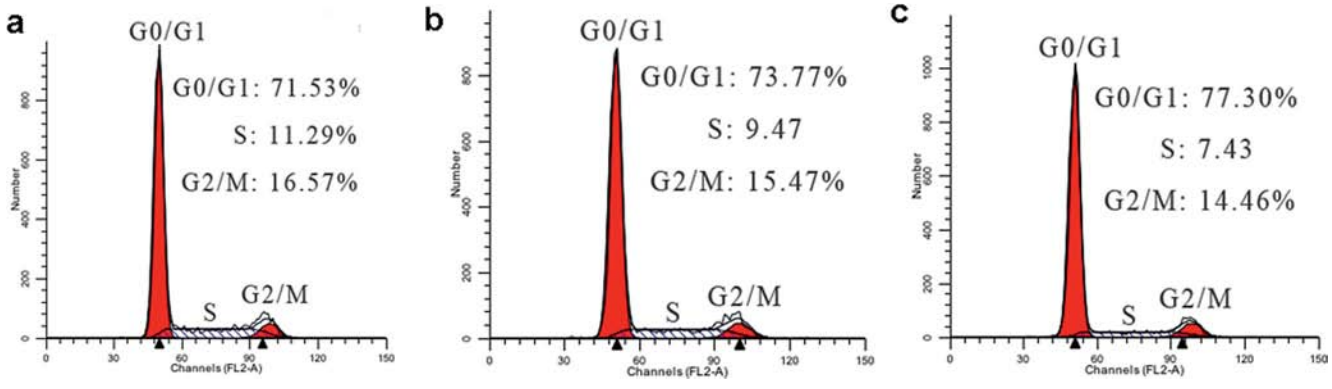

Figure 10. Cell cycle status of the MG-63 cell line after treatment with different concentrations of complex **3** for 16 h. a control, b and c for 12.5 and 25 μM, respectively.

information may be helpful in developing new potential antioxidants.

Table 3. The scavenging ratios (%) of complexes **1**, **2**, and **3** against ·OH.

	Average inhibition (%) for ·OH								
(μM)	0.5	1.0	1.5	2.0	2.5	3.0	3.5	4.0	4.5
1	2.65	10.12	27.23	44.10	56.39	59.52	61.20	68.19	75.18
2	3.86	7.95	19.52	40.24	46.02	55.66	62.17	66.51	71.81
3	4.34	16.14	27.47	37.11	53.25	61.45	71.33	78.07	79.28

Conclusions

Three new ruthenium(II) polypyridyl complexes $[Ru(dmp)_2(dcdppz)]^{2+}$ **1**, $[Ru(phen)_2(dcdppz)]^{2+}$ **2**, and $[Ru(dip)_2(dcdppz)]^{2+}$ **3** have been synthesized and characterized. The DNA-binding behaviors show that the three complexes interact with CT-DNA by intercalative mode. Upon irradiation, complexes **1**, **2**, and **3** can cleave pBR322 DNA. At high concentration, these complexes can effectively condense pGL3 plasmid DNA. The cytotoxicity assay indicates that complexes **1** and **3** exhibit higher cytotoxicity than cisplatin on Hela and HepG-2 cells. The apoptotic study shows that the three complexes can effectively induce the apoptosis of BEL-7402 cells. The flow cytometric analysis of treatment of MG-63 cells with complex **3** indicates the induction of G0/G1 phase arrest. Additionally, antioxidant activity shows that the three complexes may be potential drugs for the elimination of the hydroxy radical.

Experimental Section

Abbreviations: dcdppz: 7,8-dichlorodipyrido[3,2-*a*:2′,3′-*c*]phenazine, dmp: 2,9-dimethyl-1,10-phenanthroline, phen: 1,10-phenanthroline, dip: 4,7-diphenyl-1,10-phenanthroline, MTT: 3-(4,5-dimethylthiazol-2-yl)-2,5-diphenyltetrazolium bromide, AO: acridine orange, EB: ethidium bromide, DMSO: dimethyl sulfoxide, RPMI: Roswell Park Memorial Institute, DMF: *N*,*N*-dimethylformamide, CT DNA: calf thymus DNA, MLCT: metal-to-ligand charge transfer, Tris: tris(hydroxymethyl)aminomethane, ES-MS: electrospray mass spectroscopy.

Materials and Methods: Calf thymus DNA (CT-DNA) was obtained from the Sino-American Biotechnology Company. pBR322 DNA was obtained from Shanghai Sangon Biological Engineering & Services Co., Ltd. Dimethyl sulfoxide (DMSO) and RPMI 1640 were purchased from Sigma. BEL-7402, Hela, HepG-2, and MG-63 cell lines were purchased from the American Type Culture Collection, agarose and ethidium bromide were obtained from Aldrich. $RuCl_3 \cdot xH_2O$ was purchased from Kunming Institution of Precious Metals. 1,10-Phenanthroline was obtained from Guangzhou Chemical Reagent Factory. Doubly distilled water was used to prepare buffers [5 mM Tris(hydroxymethylaminomethane)-HCl, 50 mM NaCl, pH = 7.2]. A solution of calf thymus DNA in the buffer gave a ratio of UV absorbance at 260 and 280 nm of ca. 1.8–1.9:1, indicating that the DNA was sufficiently free of protein.[32] The DNA concentration per nucleotide was determined by absorption spectroscopy using the molar absorption coefficient (6600 $M^{-1}cm^{-1}$) at 260 nm.[33]

Microanalysis (C, H, and N) was carried out with a Perkin–Elmer 240Q elemental analyzer. Fast atom bombardment (FAB) mass spectra were recorded with a VG ZAB-HS spectrometer in a 3-nitrobenzyl alcohol matrix. Electrospray mass spectra (ES-MS) were recorded with a LCQ system (Finnigan MAT, USA) using methanol as the mobile phase. The spray voltage, tube lens offset, capillary voltage, and capillary temperature were set to 4.50 kV, 30.00 V, 23.00 V, and 200 °C, respectively, and the quoted *m*/*z* values are for the major peaks in the isotope distribution. ^{1}H NMR spectra were recorded with a Varian-500 spectrometer. All chemical shifts were given relative to tetramethylsilane (TMS). UV/Vis spectra were recorded with a Shimadzu UV-3101PC spectrophotometer and emission spectra were recorded with a Shimadzu RF-4500 luminescence spectrometer at room temperature.

Synthesis of Ligand and Complexes

Ligand (dcdppz): A mixture of 1,10-phenanthroline-5,6-dione (0.420 g, 2.0 mmol)[34] and 4,5-dichloro-1,2-phenylenediamine (0.354 g, 2.0 mmol) in ethanol (80 cm^3) was refluxed with stirring for 6 h. The cooled solution was filtered and washed with cool ethanol. An earth yellow precipitate was obtained; yield 82%. $C_{18}H_8Cl_2N_4$ (351.19): calcd. C 61.56, H 2.30, N 15.95; found C 61.39, H 2.45, N 15.76. ES–MS: m/z (%) = 352.3 $[M + H]^+$. ^{1}H NMR (500 MHz, $CDCl_3$): δ = 9.52 (dd, J = 8.0, J = 7.8 Hz, 2 H, H_c), 9.28 (dd, J = 7.6, J = 7.5 Hz, 2 H, H_a), 8.45 (s, 2 H, H_g), 7.78 (dd, J = 5.6, J = 5.5 Hz, 2 H, H_b) ppm. ^{13}C NMR (500 MHz, $CDCl_3$): δ = 153.05 C (a), 148.59 C (f), 141.91 C (i), 140.94 C (h), 135.49 C (c), 133.81 C (g), 129.87 C (d), 127.04 C (e), 124.27 C (b) ppm.

$[Ru(dmp)_2(dcdppz)](ClO_4)_2 \cdot 2CH_3CN \cdot 1.5H_2O$ (1): A mixture of *cis*-$[Ru(dmp)_2Cl_2] \cdot 2H_2O$ (0.286 g, 0.5 mmol)[35] and dcdppz (0.176 g, 0.5 mmol) in ethylene glycol (20 cm^3) was refluxed under argon for 8 h to give a clear red solution. Upon cooling, a red precipitate was obtained by dropwise addition of saturated aqueous $NaClO_4$ solution. The crude product was purified by column chromatography on a neutral alumina with a mixture of CH_3CN/toluene (3:1, v/v) as eluent. The main red band was collected. The solvent was removed under reduced pressure and a red powder was obtained; yield 70%. $C_{46}H_{32}Cl_4N_8O_8Ru \cdot 2CH_3CN \cdot 1.5H_2O$: calcd. C 51.03, H 3.51, N 11.90; found C 51.14, H 3.48, N 11.87. ES-MS $[CH_3CN]$: *m*/*z* (%) = 967.5 $([M - ClO_4]^+)$, 867.1 $([M - 2ClO_4 - H]^+)$, 434.3 $([M–2ClO_4]^{2+})$. ^{1}H NMR (500 MHz, $[D_6]$DMSO): δ = 9.36 (dd, J = 6.5, J = 4.5 Hz, 2 H, H_c), 9.43 (d, J = 8.5 Hz, 2 H, H_a), 8.77 (s, 4 H), 8.45 (dd, J = 8.0, J = 8.5 Hz, 4 H, $H_{4,7}$), 8.26 (d, J = 8.5 Hz, 1 H, H_g), 7.99 (d, J = 8.0 Hz, 1 H, H_k), 7.63 (dd, J = 6.0, J = 5.5 Hz, 2 H, H_3), 7.54 (dd, J = 5.5, J = 5.0 Hz, 2 H, H_8), 7.42 (d, J = 8.5 Hz, 2 H, H_b), 2.51 (s, 12 H) ppm. ^{13}C NMR (500 MHz, $CDCl_3$): δ = 166.89 C (2,9), 165.66 C (a), 153.02 C (f), 150.32 C (i), 147.62 C (11), 146.38 C (c), 140.15 C (h,j), 139.33 C (4,7), 137.13 C (g,k), 135.54 C (d), 133.99 C (e), 132.37 C (10), 128.40 C (5,6), 126.31 C (b), 125.73 C (3,8), 24.94 C (Me) ppm.

$[Ru(phen)_2(dcdppz)](ClO_4)_2 \cdot 2H_2O$ (2): This complex was synthesized in an identical manner as that described for complex **1**, with *cis*-$[Ru(phen)_2Cl_2] \cdot 2H_2O$[36] in place of *cis*-$[Ru(dmp)_2Cl_2] \cdot 2H_2O$; yield 71%. $C_{42}H_{24}Cl_4N_8O_8Ru \cdot 2H_2O$: calcd. C 48.15, H 2.69, N 10.70; found C 48.27, H 2.64, N 10.77. ES-MS $[CH_3CN]$: m/z (%) = 911.5 $([M–ClO_4]^+)$, 407.3 $([M–2ClO_4]^{2+})$. ^{1}H NMR (500 MHz, $[D_6]$DMSO): δ = 9.53 (dd, J = 7.0, J = 6.5 Hz, 2 H, H_c), 8.86 (t, J = 4.5 Hz, 2 H, H_a), 8.81 (dd, J = 7.0, J = 6.5 Hz, 4 H, $H_{4,7}$), 8.41 (s, 4 H, $H_{5,6}$), 8.28 (dd, J = 5.5, J = 5.0 Hz, 2 H, H_2), 8.22 (dd, J = 5.0, J = 4.5 Hz, 2 H, H_9), 8.06 (d, J = 5.0, J = 5.0 Hz, 2 H, $H_{g,k}$), 7.93 (dd, J = 5.5, J = 5.5 Hz, 2 H, H_b), 7.82 (dd, J = 5.5, J =

5.5 Hz, 2 H, H_3), 7.77 (dd, J = 5.5, J = 5.0 Hz, 2 H, H_8) ppm. ^{13}C NMR ($CDCl_3$): δ = 154.40 C (2,9), 153.28 C (a), 152.67 C (f), 150.99 C (i), 147.12 C (11), 141.15 C (c), 140.63 C (h,j), 136.99 C (4,7), 135.32 C (g,k), 133.19 C (d), 130.46 C (e), 129.67 C (10), 128.06 C (5,6), 127.70 C (b), 126.35 C (3,8) ppm.

$[Ru(dip)_2(dcdppz)](ClO_4)_2·2H_2O$ (3): This complex was synthesized in an identical manner as that described for complex **1**, with *cis*-$[Ru(dip)_2Cl_2]·2H_2O$[37] in place of *cis*-$[Ru(dmp)_2Cl_2]·2H_2O$; yield 70%. $C_{66}H_{40}Cl_4N_8O_8Ru·2H_2O$: calcd. C 58.63, H 3.28, N 8.29; found C 58.51, H 3.22, N 8.36. ES-MS [CH_3CN]: m/z (%) = 1217.00 ($[M - ClO_4]^+$), 558.4 ($[M–2ClO_4]^{2+}$). ^1H NMR (500 MHz, [D_6]DMSO): δ = 9.59 (d, J = 8.0 Hz, 2 H, H_c), 8.87 (dd, J = 4.5 Hz, 2 H, H_a), 8.39 (t, J = 5.5 Hz, 4 H, $H_{2,9}$), 8.34 (d, J = 6.0 Hz, 2 H, H_g), 8.28 (s, 4 H, $H_{5,6}$), 8.05 (dd, J = 5.5, J = 5.0 Hz, 2 H, H_b), 7.83 (dd, J = 5.0 Hz, 4 H, $H_{3,8}$), 7.59–7.71 (m, 20 H) ppm. ^{13}C NMR ($CDCl_3$): δ = 153.29 C (2,9,a), 151.62 C (4,7), 149.85 C (f), 147.00 C (i), 146.85 C (11), 140.03 C (c), 139.59 C (h,j), 134.26 C (12), 132.27 C (d, g), 129.00 C (e), 128.72 C (14,15), 128.03 C (5,6), 127.10 C (10), 126.97 C (13), 125.19 C (b), 124.89 C (3,8) ppm.

Caution: Perchlorate salts of metal compounds with organic ligands are potentially explosive, and only small amounts of the material should be prepared and handled with great care.

Crystal Structure Determination and Refinement of Complex 1: X-ray diffraction measurements were performed with a Bruker Smart CCD area detector in the range $1.5 < \theta < 26°$ with Mo-K_α radiation (λ = 0.71073 Å) at 120 K. All empirical absorption corrections were applied by using the SADABS program.[38] The structures were determined using pattern methods, which yielded the positions of all non-hydrogen atoms. All the hydrogen atoms of the complexes were placed in calculated positions with fixed isotropic thermal parameters and the structure factor calculations were included in the final stage of full-matrix least-squares refinement. All calculations were performed using the SHELXTL-97 suite of the computer programs.[39] For data see Table 4.

Table 4. Crystal data for complex **1**.

	$C_{46}H_{32}Cl_2N_8O_8Ru·2CH_3CN·1.5H_2O$
M_r	2363.60
T [K]	120
λ [Å]	0.71073
Crystal system	monoclinic
Space group	*C*2/*c*
a [Å]	18.454(3)
b [Å]	44.648(7)
c [Å]	13.082(2)
α [°]	90
β [°]	99.911(3)
γ [°]	90
V [Å^3]	10618(3)
Z	4
D_c [g cm^{-1}]	1.472
Crystal size [mm]	0.22 × 0.24 × 0.28
θ range for data collection [°]	1.82–26.00
Limiting indices, *hkl*	–22 to 21, –45 to 55, –16 to 8
Reflections collected	10315
Independent reflections (R_{int})	8068
Good-of-fit on F^2	1.088
R_1/wR_2 [$I > 2\sigma(I)$][a]	0.0563/0.1150
R_1/wR_2 (all data)[a]	0.0730/0.1190
Largest diff. peak [e Å^{-1}]	0.38/–0.40

[a] $R_1 = \Sigma||F_o| - |F_c||/\Sigma|F_o|$, $wR_2 = [\Sigma w(F_o^2 - F_c^2)^2/\Sigma w(F_o^2)^2]^{1/2}$.

DNA Binding and Photoactivated Cleavage: The DNA-binding and photoactivated cleavage experiments were performed at room temperature. Buffer A [5 mM tris(hydroxymethyl)aminomethane (Tris) hydrochloride, 50 mM NaCl, pH 7.0] was used for absorption titration, luminescence titration, and viscosity measurements. Buffer B (50 mM Tris-HCl, 18 mM NaCl, pH 7.2) was used for DNA photocleavage experiments. Buffer C (0.9% of physiological saline) was used for the retardation assay of pGL 3 plasmid DNA.

The absorption titrations of the complex in buffer were performed using a fixed concentration (20 μM) for each complex to which increments of the DNA stock solution were added. Ru–DNA solutions were allowed to incubate for 5 min before the absorption spectra were recorded. The intrinsic binding constants K, based on the absorption titration, were measured by monitoring the changes of absorption in the MLCT band with increasing concentration of DNA using the following equation.[40]

$$(\varepsilon_a - \varepsilon_f)/(\varepsilon_a - \varepsilon_f) = b - (b^2 - 2K^2C_t[\mathrm{DNA}]/s)^{1/2}/2KC_t \quad (1a)$$

$$b = 1 + KC_t + K[\mathrm{DNA}]/2s \quad (1b)$$

where [DNA] is the concentration of CT-DNA in base pairs, the apparent absorption coefficients ε_a, ε_f, and ε_b correspond to A_{obsed}/[Ru], the absorbance for the free ruthenium complex, and the absorbance for the ruthenium complex in fully bound form, respectively. K is the equilibrium binding constant, C_t is the total metal complex concentration in nucleotides and s is the binding site size.

Binding stoichiometries were obtained for complexes **2** and **3** with CT-DNA using the method of continuous variation.[16] The concentrations of the three complexes and DNA were varied, while the sum of the reactant concentrations was kept constant at 50 μM (in terms of base pairs for the DNA). Solutions of complexes and DNA were prepared in Tris-HCl buffer (pH = 7.4). In the sample solutions, the mol fraction χ of the complex was varied from 0 to 1.0 in 0.1 ratio steps. The luminescence intensities of these mixtures were measured at 25 °C using an excitation wavelength of 460 nm. The fluorescence intensity was plotted vs. the mol fraction χ of the complex to generate a Job plot. Linear regression analysis of the data was performed with the Origin 7.0 software.

Viscosity measurements were carried out using an Ubbelodhe viscometer maintained at a constant temperature of 25.0 (± 0.1) °C in a thermostatic bath. DNA samples approximately 200 base pairs in average length were prepared by sonication to minimize complexities arising from DNA flexibility.[41] Flow time was measured with a digital stopwatch, and each sample was measured three times, and an average flow time was calculated. Relative viscosities for DNA in the presence and absence of the complexes were calculated from the relation $\eta = (t - t^0)/t^0$, where t is the observed flow time of the DNA-containing solution and t^0 is the flow time of buffer alone.[42,43] Data were presented as $(\eta/\eta_0)^{1/3}$ vs. binding ratio,[44] where η is the viscosity of DNA in the presence of complexes and η_0 is the viscosity of DNA alone.

For the gel electrophoresis experiment, supercoiled pBR 322 DNA (0.1 μg) was treated with the Ru^{II} complexes in buffer B, and the solution was then irradiated at room temperature with a UV lamp (365 nm, 10 W). The samples were analyzed by electrophoresis for 1.0 h at 80 V on a 0.8-% agarose gel in TBE (89 mM Tris-borate acid, 2 mM EDTA, pH = 8.3). The gel was stained with 1 μg mL^{-1} ethidium bromide and photographed on an Alpha Innotech IS-5500 fluorescence chemiluminescence and visible imaging system.

Cytotoxicity Assay in Vitro: Standard 3-(4,5-dimethylthiazole)-2,5-diphenyltetraazolium bromide (MTT) assay procedures were

used.[45] Cells were placed in 96-well microassay culture plates (8×10^3 cells per well) and grown overnight at 37 °C in a 5-% CO_2 incubator. Compounds tested were then added to the wells to achieve final concentrations ranging from 10^{-6} to 10^{-4} M. Control wells were prepared by addition of culture medium (100 μL). The plates were incubated at 37 °C in a 5-% CO_2 incubator for 72 h. Upon completion of the incubation, stock MTT dye solution (20 μL, 5 mg mL^{-1}) was added to each well. After 4 h, buffer (100 μL) containing *N*,*N*-dimethylformamide (50%) and sodium dodecyl sulfate (20%) was added to solubilize the MTT formazan. The optical density of each well was then measured with a microplate spectrophotometer at a wavelength of 490 nm. The IC_{50} values were determined by plotting the percentage viability vs. concentration on a logarithmic graph and reading off the concentration at which 50% of cells remain viable relative to the control. Each experiment was repeated at least three times to obtain the mean values. Four different tumor cell lines were the subjects of this study: BEL-7402 (Human hepatocellular carcinoma cell line), Hela (Human epithelial carcinoma cell line), HepG-2 (Human hepatocellular carcinoma cell line), and MG-63 (Human osteosarcoma cell line), and these cells were purchased from the American Type Culture Collection (Rockville, MD).

Apoptosis Assessment by AO/EB Staining: Apoptosis studies were performed with a staining method utilizing acridine orange (AO) and ethidium bromide (EB).[28] AO can pass through cell membranes, but EB cannot. Under the fluorescence microscope, living cells appear green. Necrotic cells stain red but have a nuclear morphology resembling that of viable cells. Apoptotic cells appear green, and morphological changes such as cell blebbing and formation of apoptotic bodies will be observed. A monolayer of BEL-7402 cells was incubated in the absence and presence of complex **3** at a concentration of 25 μM at 37 °C and 5% CO_2 for 24 h. Then each cell culture was stained with AO/EB solution (100 μg mL^{-1} AO, 100 μg mL^{-1} EB). Samples were observed under a fluorescence microscope.

Flow Cytometric Analysis: MG-63 cells were seeded into six-well plates (Costar, Corning Corp, New York) at a density of 2×10^5 cells per well and incubated for 16 h. The cells were cultured in RPMI 1640 supplemented with fetal bovine serum (FBS, 10%) and incubated at 37 °C and 5% CO_2. The medium was removed and replaced with medium (final DMSO concentration, 1% v/v) containing complex **3** (12.5 and 25 μM). After incubation for 16 h, the cell layer was trypsinized and washed with cold PBS (phosphate buffered saline) and fixed with 70% ethanol. 20 mL of RNAse (0.2 mg/mL) and 20 mL of propidium iodide (0.02 mg/mL) were added to the cell suspensions and they were incubated at 37 °C for 30 min. Then the samples were analyzed with a FACSCalibur flow cytometer (Becton Dickinson & Co., Franklin Lakes, NJ). The number of cells analyzed for each sample was 10000.[46]

Scavenger Measurements of Hydroxy Radical (·OH): The solution of the tested complexes was prepared with DMF (*N*,*N*-dimethylformamide). The assay mixture (5 mL) contained the following reagents: safranin (28.5 μM), EDTA-Fe^{II} (100 μM), H_2O_2 (44.0 μM), the tested compounds (0.5–4.5 μM), and a phosphate buffer (67 mM, pH = 7.4). The assay mixtures were incubated at 37 °C for 30 min in a water bath. Then the absorbance was measured at 520 nm. All tests were run in triplicate and expressed as the mean. A_i was the absorbance in the presence of the tested compound; A_0 was the absorbance in the absence of the tested compounds; A_c was the absorbance in the absence of the tested compound, EDTA-Fe^{II} and H_2O_2. The suppression ratio (η_a) was calculated on the basis of $(A_i - A_0)/(A_c - A_0) \times 100\%$.

CCDC-839716 contains the supplementary crystallographic data (excluding structure factors) for the structures reported in this work. These data can be obtained free of charge from the Cambridge Crystallographic Data Centre via www.ccdc.cam.ac.uk/data_request/cif.

Acknowledgments

This work was financially supported by the National Nature Science Foundation of China (grant numbers 30800227, 31070858) and Guangdong Pharmaceutical University.

[1] J. Sun, Y. An, L. Zhang, H. Y. Chen, Y. Han, Y. J. Wang, Z. W. Mao, L. N. Ji, *J. Inorg. Biochem.* **2011**, *105*, 149–154.
[2] S. Shi, X. T. Geng, J. Zhao, T. M. Yao, C. R. Wang, D. J. Yang, L. F. Zheng, L. N. Ji, *Biochimie* **2010**, *92*, 370–377.
[3] U. Schatzschneider, J. Niesel, I. Ott, R. Gust, H. Alborzinia, S. Wölfl, *ChemMedChem* **2008**, *3*, 1104–1109.
[4] C. A. Puckett, J. K. Barton, *J. Am. Chem. Soc.* **2007**, *129*, 46–47.
[5] C. A. Puckett, J. K. Barton, *Biochemistry* **2008**, *47*, 11711–11716.
[6] J. G. Liu, Q. L. Zhang, X. F. Shi, L. N. Ji, *Inorg. Chem.* **2001**, *40*, 5045–5050.
[7] C. P. Tan, S. S. Lai, S. H. Wu, S. Hu, L. J. Zhou, Y. Chen, M. X. Wang, Y. P. Zhu, W. Lian, W. L. Peng, L. N. Ji, A. L. Xu, *J. Med. Chem.* **2010**, *53*, 7613–7624.
[8] J. Breu, A. J. Stoll, *Acta Crystallogr., Sect. C* **1996**, *52*, 1174–1177.
[9] Y. J. Liu, C. H. Zeng, J. H. Yao, F. H. Wu, L. X. He, H. L. Huang, *Chem. Biodiversity* **2010**, *7*, 1770–1783.
[10] S. Satyanarayana, J. C. Dabrowiak, J. B. Chaires, *Biochemistry* **1993**, *32*, 2573–2584.
[11] H. J. Yu, S. M. Huang, L. Y. Li, H. N. Ji, H. Chao, Z. W. Mao, J. Z. Liu, L. N. Ji, *J. Inorg. Biochem.* **2009**, *103*, 881–890.
[12] Y. J. Liu, X. Y. Wei, F. H. Wu, W. J. Mei, L. X. He, *Spectrochim. Acta Part A* **2008**, *70*, 171–176.
[13] S. Shi, J. Liu, J. Li, K. C. Zheng, C. P. Tan, L. M. Chen, L. N. Ji, *Dalton Trans.* **2005**, 2038–2046.
[14] J. E. Coury, J. R. Anderson, L. McFail-Isom, L. D. Williams, L. A. Bottmley, *J. Am. Chem. Soc.* **1997**, *119*, 3792–3796.
[15] F. Gao, X. Chen, J. Q. Wang, Y. Chen, H. Chao, L. N. Ji, *Inorg. Chem.* **2009**, *48*, 5599–5601.
[16] P. Job, *Ann. Chim. (Paris)* **1928**, *9*, 113–203.
[17] J. K. Barton, A. L. Raphael, *J. Am. Chem. Soc.* **1984**, *106*, 2466–2468.
[18] H. L. Huang, Y. J. Liu, C. H. Zeng, L. X. He, F. H. Wu, *DNA Cell Biol.* **2010**, *29*, 261–270.
[19] L. F. Tan, J. L. Shen, X. J. Chen, X. L. Liang, *DNA Cell Biol.* **2009**, *28*, 461–468.
[20] H. L. Huang, Z. Z. Li, Z. H. Liang, Y. J. Liu, *Eur. J. Med. Chem.* **2011**, *46*, 3282–3290.
[21] S. A. Allison, J. C. Herr, J. M. Schurr, *Biopolymers* **1981**, *20*, 469–488.
[22] J. Widom, R. L. Baldwin, *Biopolymers* **1983**, *22*, 1595–1620.
[23] T. J. Thomas, V. A. Bloomfield, *Biopolymers* **1983**, *22*, 1097–1106.
[24] B. Sun, J. X. Guan, L. Xu, B. L. Yu, L. Jiang, J. F. Kou, L. Wang, X. D. Ding, H. Chao, L. N. Ji, *Inorg. Chem.* **2009**, *48*, 4637–4639.
[25] Y. J. Liu, C. H. Zeng, Z. H. Liang, J. H. Yao, H. L. Huang, Z. Z. Li, F. H. Wu, *Eur. J. Med. Chem.* **2010**, *45*, 3087–3095.
[26] T. F. Chen, Y. N. Liu, W. J. Zheng, J. Liu, Y. S. Wong, *Inorg. Chem.* **2010**, *49*, 6366–6368.
[27] A. Martínez, C. S. K. Rajapakse, R. A. Sánchez-Delgado, A. Varela-Ramirez, C. Lema, R. J. Aguilera, *J. Inorg. Biochem.* **2010**, *104*, 967–977.

[28] D. L. Spector, R. D. Goldman, L. A. Leinwand (Eds.), *Cells: A Laboratory Manual*, Cold Spring Harbor Laboratory Press, New York, **1998**, Vol. 1, Chapter 15.
[29] P. Valentao, E. Fernandes, F. Carvalho, P. B. Andrade, R. M. Seabra, M. L. Bastos, *Biol. Pharm. Bull.* **2002**, *25*, 1320–13323.
[30] B. Bektasoglu, S. E. Celik, M. Ozyurek, K. Guclu, R. Apak, *Biochem. Biophys. Res. Commun.* **2006**, *345*, 1194–1200.
[31] C. C. Cheng, S. E. Rokita, C. J. Burrows, *Angew. Chem.* **1993**, *105*, 290; *Angew. Chem. Int. Ed. Engl.* **1993**, *32*, 277–278.
[32] J. Marmur, *J. Mol. Biol.* **1961**, *3*, 208–218.
[33] M. E. Reichmann, S. A. Rice, C. A. Thomas, P. Doty, *J. Am. Chem. Soc.* **1954**, *76*, 3047–3053.
[34] M. Yamada, Y. Tanaka, Y. Yoshimoto, S. Kuroda, I. Shimao, *Bull. Chem. Soc. Jpn.* **1992**, *65*, 2007–2009.
[35] J. P. Collin, J. P. Sauvage, *Inorg. Chem.* **1986**, *25*, 135–141.
[36] B. P. Sullivan, D. J. Salmon, T. J. Meyer, *Inorg. Chem.* **1978**, *17*, 3334–3341.
[37] R. Caspar, C. Cordier, J. B. Waern, C. Guyard-Duhayon, M. Gruselle, P. L. Floch, H. Amouri, *Inorg. Chem.* **2006**, *45*, 4071–4078.
[38] G. M. Sheldrick, *SADABS*, *Program for Empirical Absorption Correction of Area Detector Data*, University of Göttingen, Germany, **1996**.
[39] G. M. Sheldrick, *SHELXL-97*, *Program for Crystal Structure Refinement*, University of Göttingen, Germany, **1997**.
[40] M. T. Carter, M. Rodriguez, A. Bard, *J. Am. Chem. Soc.* **1989**, *111*, 8901–8911.
[41] J. B. Chaires, N. Dattagupta, D. M. Crothers, *Biochemistry* **1982**, *21*, 3933–3940.
[42] S. Satyanarayana, J. C. Dabrowiak, J. B. Chaires, *Biochemistry* **1993**, *32*, 2573–2584.
[43] S. Satyanaryana, J. C. Dabrowial, J. B. Chaires, *Biochemistry* **1992**, *31*, 9319–9324.
[44] G. Cohen, H. Eisenberg, *Biopolymers* **1969**, *8*, 45–55.
[45] T. Mosmann, *J. Immunol. Methods* **1983**, *65*, 55–63.
[46] K. K. Lo, T. K. Lee, J. S. Lau, W. L. Poon, S. H. Cheng, *Inorg. Chem.* **2008**, *47*, 200–208.

Received: August 13, 2011
Published Online: November 10, 2011

